
Article:
Montefiori, E. orcid.org/0000-0003-2498-7877, Hayford, C.F. and Mazzà, C. (2022) Variations of lower-limb joint kinematics associated with the use of different ankle joint models. Journal of Biomechanics, 136. 111072. ISSN 0021-9290

https://doi.org/10.1016/j.jbiomech.2022.111072

Journal of Biomechanics 136 (2022) 111072

Contents lists available at ScienceDirect

Journal of Biomechanics

journal homepage: www.elsevier.com/locate/jbiomech

Variations of lower-limb joint kinematics associated with the use of different ankle joint models

Erica Montefiori [a,b], Claude Fiifi Hayford [a,b], Claudia Mazzà [a,b]

[a] INSIGNEO Institute for in silico Medicine, The University of Sheffield, Sheffield, UK
[b] Department of Mechanical Engineering, The University of Sheffield, Sheffield, UK

ARTICLE INFO

Keywords:
Ankle
Inverse kinematics
Joint kinematics
Juvenile
Modelling
MRI
OpenSim
Subtalar
Tibiotalar

ABSTRACT

Skeletal computational models relying on global optimisation are widely used alongside gait analysis for the estimate of joint kinematics, but the degrees of freedom (DOFs) and axes definitions to model the ankle complex are still debated. The aim of this paper is to establish whether ankle modelling choices would also critically affect the estimate of the other joints' kinematics. Gait and MRI data from fifteen juvenile participants were used to implement three ankle joint models (M1, one-DOF sagittal motion; M2, two-DOFs sagittal and frontal motions; M3, three-DOFs) as part of a full lower-limb skeletal model. Differences in lower-limb joint and foot progression angles calculated using global optimisation were evaluated both at individual and group level. Furthermore, the influence of these differences on the correlations between joints and on the calculations of the root mean square deviation (RMSD) were investigated. Inter-model variations at individual level reached up to 4.2°, 9.1°, and 15.0° for hip flexion, adduction, and rotation, respectively, and up to 6.5° for knee flexion. Despite the tibiotalar axis being the same for all models, up to 19.3° (9.1° on average) larger dorsiflexion was found at push-off with M2. A stronger correlation between foot progression and ankle and knee sagittal movements was found for M1. Finally, RMSD led to inconsistent ranking of the participants when using different models. In conclusion, the choice of the ankle joint model affects the estimates of proximal lower-limb joint kinematics, which should discourage comparisons across datasets built with different models.

1. Introduction

Skeletal computational models driven by global optimisation (Lu and O'connor, 1999) are well established alongside gait analysis for the estimate of joint kinematics. A critical point in the specification of skeletal models is the level of detail in the definition of the articulating joints: different degrees of biofidelity with the joint physiological function can be achieved depending on both the purpose of the investigation and the quality of the input data. When constructed from medical images, such as magnetic resonance imaging (MRI), these models can provide a more accurate description of the skeletal system of a specific individual (Ding et al., 2019; Smith et al., 1989) and support the assessment of locomotory function in both healthy and pathological scenarios (Montefiori et al., 2019).

Modelling of the ankle joint complex, comprised of the tibiotalar (between tibia and talus) and subtalar (between talus and calcaneus) joints, has received increased attention in recent times due to its key role in human locomotion. Although general guidelines have been proposed and agreed for modelling the main joints of the lower limb (Wu et al., 2002), new and more complex ankle joint models are presented and validated almost yearly (de Asla et al., 2006; Kleipool et al., 2019; Maharaj et al., 2020). A recent review (Lenz et al., 2021) identified 52 papers published between 2006 and 2020 proposing image-based models of the tibiotalar and subtalar joints.

When static imaging data are available, the ankle is commonly represented by simple ideal hinges to separately describe the tibiotalar and subtalar joints (Malaquias et al., 2017; Montefiori et al., 2019; Roach et al., 2016), or one ideal ball-and-socket joint that describes its three rotational degrees of freedom (DOFs) (Prinold et al., 2016; Saraswat et al., 2010). More accurate definitions are possible if tools like biplane fluoroscopy or weightbearing computed tomography are available to independently quantify the six-DOF kinematics of the tibiotalar and subtalar joints (Wang et al., 2015). Besides differing in terms of their fidelity and accuracy, these models intrinsically differ both for number of DOFs and axes orientation.

When adopting different modelling approaches, the estimates of ankle kinematics can change dramatically. For example, up to 15° of difference was found when comparing tibiotalar kinematics from one-DOF and three-DOF ankle models (Nichols et al., 2016). The effect of these changes might propagate to the other joints in the kinematic chain, such as the knee or the hip. A few clinical studies have quantified the relationship between foot kinematics and pelvis alignment, but mostly

https://doi.org/10.1016/j.jbiomech.2022.111072
Accepted 25 March 2022
Available online 2 April 2022

within pathological scenarios and in static conditions (Khamis and Yizhar, 2007; Pinto et al., 2008). Kainz et al. (2017b) showed that kinematic models with different knee and ankle DOFs produce significantly different estimates of pelvis and hip kinematics. However, to the best of our knowledge, no study has investigated the effect that adopting different ankle models has on the estimates of the proximal lower-limb joint kinematics during gait.

Patients with abnormal ankle kinematics typically present compensatory alterations in their hip and pelvis kinematics (Khamis and Yizhar, 2007). Nonetheless, the potential effect that different representations of the various joint axes can have on the quantification and interpretation of these inter-joint compensations has not yet been fully investigated. Specifically, it is unclear if different definitions of the ankle joint would provide different estimates of knee, hip, and pelvis kinematics, although it could be hypothesised that accounting for non-sagittal foot movements by increasing the number of DOFs would have a particular effect on the non-sagittal rotations of the proximal joints of the limb (i.e. hip and pelvis). If this was true, the specific modelling choice would represent a significant confounding factor for the clinical interpretation. The aim of this study was hence to quantify the effect of varying the joint DOFs and joint axes orientations at the ankle on the estimate of the lower-limb joint kinematics.

2. Methods

2.1. Subjects and data

Data from fifteen juvenile participants (4:11 males:females, age: 12 ± 3 years, mass: 47.2 ± 15.8 kg, height: 1.46 ± 0.20 m) were retrospectively selected from those recruited as part of a EU-funded project (MD-Paedigree, 7th FP, Contract Number 600932, Ethics approval AM IGG 01 2013) investigating juvenile idiopathic arthritis. Inclusion criteria required confirmed joint integrity, sound joint functioning and exclusion of gait alterations according to a rheumatologist examination based on assessment of bone, cartilage and tendons on medical images (details in Montefiori et al. (2019)). Gait data were collected across two laboratories (Istituto Giannina Gaslini, Genoa, and Ospedale Pediatrico Bambin Gesù, Rome) using a stereophotogrammetric system (6-camera BTS, Smart DX, 100 Hz and 8-camera, ViconMX, 200 Hz). The participants were asked to walk across the laboratory at self-selected speed until three trials were recorded in which all markers were visible. The marker set was a combination of the Vicon Plugin-Gait (Vicon Motion System) and the modified Oxford Foot Model (Stebbins et al., 2006), for a total of twenty markers on each limb (thirteen on the foot). All gait markers were replaced by MRI-visible markers for the subsequent imaging session to allow registering marker locations with skeletal geometries obtained from MRI. Imaging included a lower-limb e-THRIVE MRI scan (Philips Medical Systems, 1.5T, 1mm in-plane resolution, 1 mm slice thickness, field-of-view: FH 210 mm; AP 210 mm; RL 55 mm, repetition time: 35 ms,echo time: 9.2 ms, average scan time: 06.50', flip angle: 35°) and a regional foot and ankle multi-slice multi-echo 3D Gradient Echo (3D_mFFE_WATS) MRI scan with water-only selection in the sagittal plane (0.5 mm in-plane resolution, 1 mm slice thickness, field-of-view: FH 380 mm; AP 280 mm; RL 240 mm, repetition time: 4.4 ms, echo time: 2.2 ms, average scan time: 01.55' * 5 stacks, flip angle: 10°).

2.2. Lower limb skeletal model

Fifteen mono-lateral lower-limb skeletal models were built in NMS Builder (Valente et al., 2017). 3D bone geometries were segmented using an in-house developed statistical shape model approach based on Steger et al. (2012) from both the 3D_mFFE_WATS (foot and distal tibia) and the e-THRIVE (full tibia, femur and pelvis). Five fiducial points were virtually palpated (van Sint Jan, 2007) onto the two tibia geometries in MeshLab (Cignoni et al., 2008) and used to register proximal and distal segments by means of iterative closest point registration. The models were built according to a published pipeline (Modenese et al., 2018), except for what concerns the ankle complex (see following section). The joint axes were identified based on anatomical landmarks and bone morphology. Hip was modelled as an ideal ball-and-socket and a hinge was chosen for the knee, in line with most of the literature models relying on global optimisation (Arnold et al., 2010; Delp et al., 1990; Rajagopal et al., 2016). Ankle was modelled as described below.

2.3. Ankle skeletal models

Three ankle models were implemented, which were chosen as being those most adopted within the musculoskeletal modelling literature. Two of these models differed for the number of DOFs used to represent the ankle but both accounted for morphological constraints to define joint axes (Montefiori et al., 2019). The third one included a spherical joint (three DOFs), with the corresponding axes defined according to the functional planes of motion.

More in details, Model 1 (M1) included a 1-DOF hinge for the tibiotalar joint (Fig. 1). Morphological fitting was adopted to fit a cylinder to the superior surface of the talus segmented from the MRI (Montefiori et al., 2019). The cylinder axis was assigned as the ankle mediolateral axis, here referred to as the tibiotalar axis, permitting only flexion/extension rotations (Fig. 1).

Model 2 (M2) included the same tibiotalar axis as M1 and a 1-DOF hinge for the subtalar joint (Fig. 1), which was modelled by fitting two spheres to the antero-inferior and posterior-inferior surfaces of the talus (Montefiori et al., 2019). The axis connecting the centres of the two spheres coincided with the subtalar axis, representing an anatomically consistent eversion movement (Fig. 1).

Model 3 (M3) included a 3-DOF spherical ankle joint (Prinold et al., 2016; Saraswat et al., 2010) (Fig. 1) with the mediolateral axis (ankle flexion/extension) identified as per M1. The anteroposterior axis (inversion/eversion) was parallel to the ground (identified as the plane containing the most inferior points on the calcaneus, and the first and fifth metatarsal distal heads) and the inferosuperior axis (internal/external rotation) was found with the right-hand convention.

2.4. Simulations and data analysis

One randomly selected full gait cycle was simulated for each participant (Inverse Kinematics Tool, OpenSim3.3 (Delp et al., 2007)) to estimate the joint and foot progression angles. The latter was defined as the angle between the horizontal projection of the direction of progression of the pelvis and the line connecting the calcaneus to the second metatarsal (Rutherford et al., 2008). Marker weights were adjusted to ensure a maximum tracking error, defined as the maximum of the distances between each gait marker and the corresponding model marker at each time frame, smaller than 2 cm (Rajagopal et al., 2016).

Changes in the joint kinematics (pelvis tilt, obliquity, and rotation, hip flexion, adduction, and rotation, knee flexion, ankle dorsiflexion, and foot progression) were analysed both at participant level and at group level (average across the cohort). For each participant (p), differences between the kinematics calculated with the various models (ΔMij) were quantified by subtracting the values of the time-series ($y^{t,d}_{M,p}$) obtained by each model (M) for a certain joint angle (a) at each time frame (t) as shown in Eq (1).

$$\Delta Mij^{t,a}_{p} = y^{t,a}_{Mi,p} - y^{t,a}_{Mj,p} \quad (1)$$

Maximum differences over the gait cycle were calculated. In the group-level analysis the same quantities were used to identify general trends appearing as a result of changing models. Non-parametric time-dependent one-way repeated measures ANOVA, and associated post-hoc analysis, were conducted to compare the average kinematics of the three models (Statistical Parametric Mapping MATLAB package SPM1D

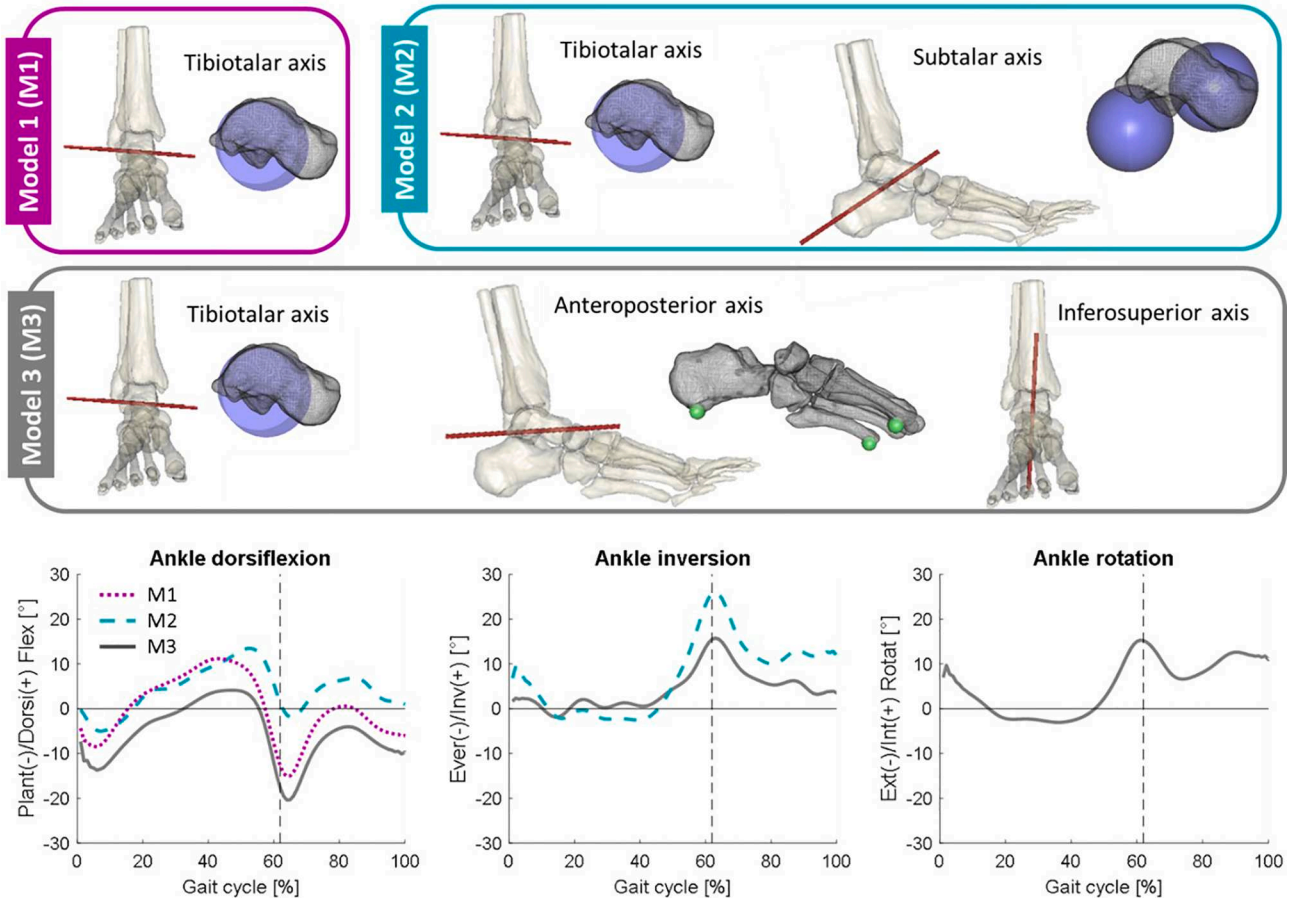

Fig. 1. Visualisation of the joint axes included in each ankle skeletal model. The tibiotalar axis for all models and the subtalar axis in Model 2 (M2) were defined based on morphological fitting. In Model 3 (M3), the anteroposterior axis was identified based on virtual palpation (van Sint Jan, 2007) of bony landmarks on the segmented foot geometries. The palpated landmarks (green dots) represent the most inferior points on calcaneus, first metatarsal and fifth metatarsal. The plane containing these three points is assumed as the ground plane and the anteroposterior axis is parallel to this plane and perpendicular to the tibiotalar axis. The inferosuperior axis was found according to the right-hand convention for cartesian systems. The bottom plots show the ankle joint kinematics for one representative participant as obtained with M1 (dotted purple), M2 (dashed turquoise) and M3 (solid grey).

(Pataky, 2012)). Cohen's *d* value allowed to quantify the effect size and assess the risk of type II errors.

Different ankle models can affect the whole limb chain by modifying the amount of crosstalk and coupling between the joints. To assess this aspect, interactions between pairs of joint angles within each model were investigated by looking at the changes in the Pearson's correlation coefficient (r) between their waveforms (MATLAB v9.10, 2021a, The MathWorks Inc., USA). Correlations were considered strong when $|r| > 0.7$, moderate when $0.5 < |r| \leq 0.7$, weak when $0.3 < |r| \leq 0.5$ and absent when $|r| \leq 0.3$, respectively. When significant values were found, the correlations obtained by the different models were compared by means of a non-parametric one-way repeated measure ANOVA (after conducting normality test). Post-hoc analysis was based on the Wilcoxon signed-rank test. Statistical significance was set to 0.05 for all tests with a Bonferroni correction for post-hoc comparisons.

For each participant (p), deviation from reference kinematic waveforms was quantified by comparing the kinematics of that participant ($y_{M,p}^{t,a}$) to the average kinematics of the remaining cohort ($y_{\overline{M}}^{t,a}$).The comparison was based on the root mean square deviation ($RMSD_{M,p}^{a}$) between $y_{M,p}^{t,a}$ and $y_{\overline{M}}^{t,a}$ for each joint angle (a) and over the duration of the whole gait cycle (T) (Eq (2)):

$$RMSD_{M,p}^{a} = \sqrt{\frac{\sum_{t=1}^{T}\left(y_{M,p}^{t,a} - y_{\overline{M}}^{t,a}\right)^2}{T}} \tag{2}$$

The average RMSD ($\overline{RMSD_{M,P}}$) was then calculated over the n = 9 considered kinematic variables (Eq. (3)):

$$\overline{RMSD_{M,P}} = \sum_{a=1}^{n} \frac{RMSD_{p}^{a}}{n} \tag{3}$$

3. Results

Maximum marker tracking errors after inverse kinematics were 1.2 ± 0.3 cm, 1.0 ± 0.2 cm, and 1.0 ± 0.2 cm for M1, M2 and M3, respectively.

Differences between models' estimates were reported in Fig. 2 for all participants as ΔM12, ΔM23, ΔM13. Maximum values for these quantities were 0.6°, 4.0°, and 0.4° for pelvis tilt, obliquity, and rotation, respectively; 4.2°, 9.1°, and 15.0° for hip flexion, adduction, and rotation, respectively; 6.5° for knee flexion. Higher values, up to 19.3° and 21.2°, were found for ankle dorsiflexion and foot progression, respectively (individual values in additional material, Table A1). Notably, the largest differences were always observed between M3 and M1, except for the ankle dorsiflexion where they occurred between M2 and M3.

When comparing the mean group kinematic curves, some statistically significant differences emerged, as shown by the post-hoc analysis results (Fig. 3). These were minimal for all pelvis movements and for the hip flexion (always below 1.6°, Table 1). At the hip, M1 significantly differed from the other models for larger adduction and internal rotations (up to 3.9° and 6.4°, respectively, with $p = 0.006$ in both cases)

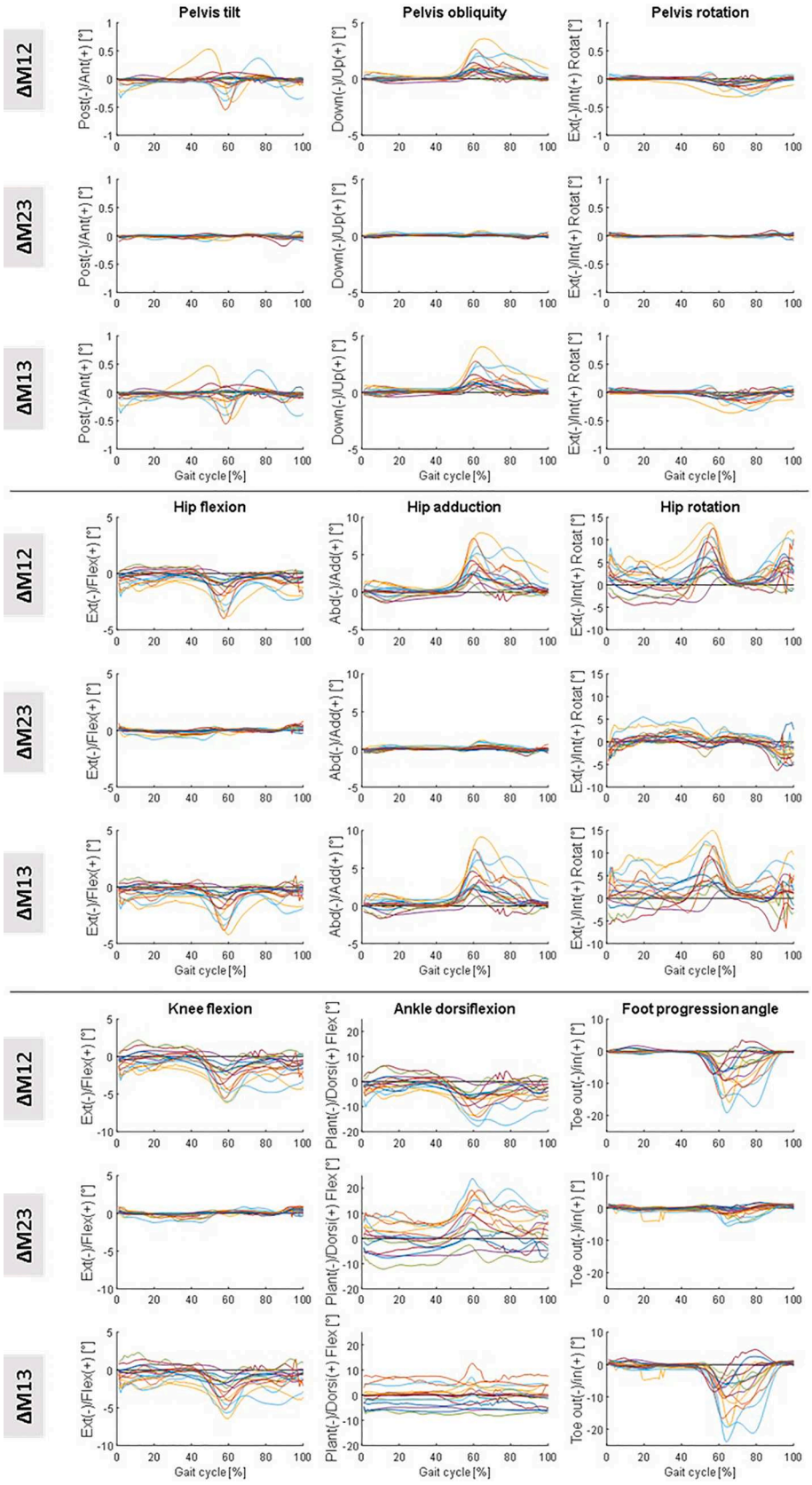

Fig. 2. Differences observed between M1 and M2 (top row), M2 and M3 (middle row), and M1 and M3 (bottom row) for the fifteen analysed cases (each line represents a participant).

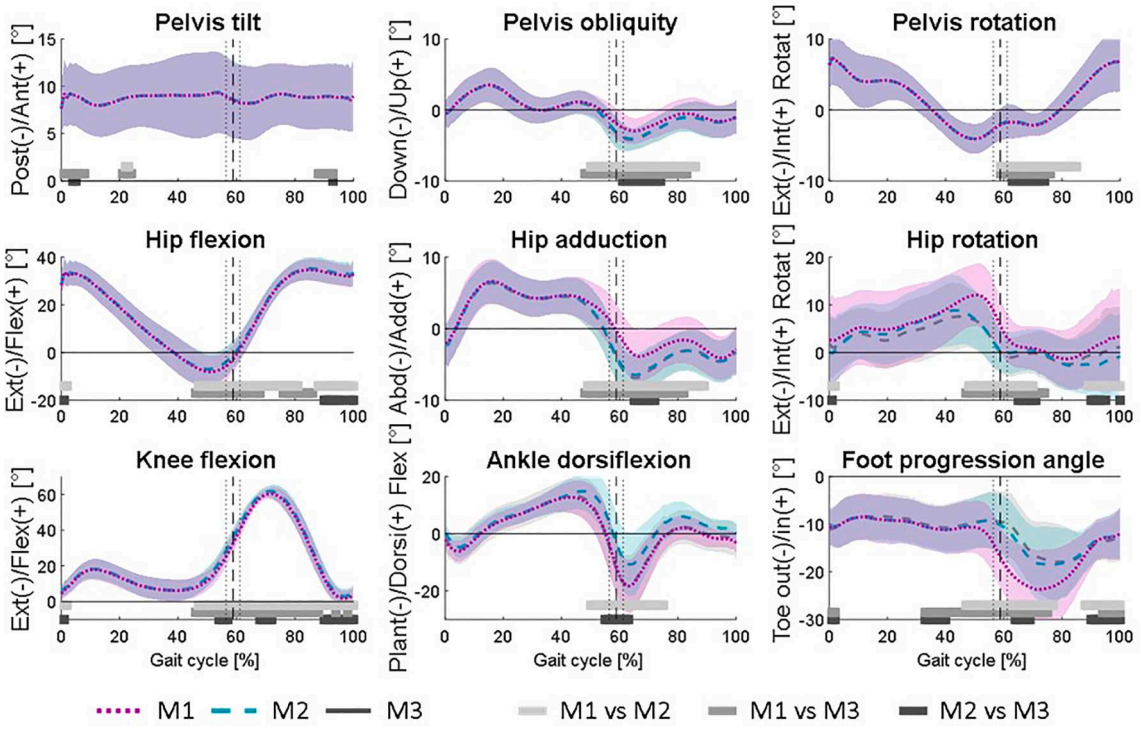

Fig. 3. Average kinematics ± 1 standard deviation across all participants for the models M1 (purple dotted), M2 (turquoise dashed), and M3 (grey solid) with statistical significance as per non-parametric post-hoc test (bottom grey bars). Vertical dashed lines indicate average toe-off instant ± 1 standard deviation.

Table 1
Group-level maximum differences (over the gait cycle) between average kinematic curves from all participants.

	Pelvis			Hip			Knee	Ankle	Foot
	tilt	obliquity	rotation	flexion	adduction	rotation	flexion	dorsiflexion	progression
ΔM12 [°]	-0.1	1.2	−0.1	−1.7	3.7	6.7	−3.2	−8.4	−8.3
ΔM23 [°]	0.0	0.1	0.0	0.3	0.4	−2.3	0.4	9.1	−1.9
ΔM13 [°]	−0.1	−1.4	0.1	−1.7	4.0	6.7	−3.1	−0.9	−10.0

ΔM12, ΔM23, and ΔM13 refer to difference (in degrees [°]) between average kinematics curves obtained with M1 and M2, M2 and M3, and M1 and M3, respectively.

during late stance and swing, while M2 showed a slightly smaller internal rotation in terminal swing and mid stance (up to 2.2°, $p = 0.006$). Similarly, a significant 3.0° smaller knee flexion was found for M1 ($p = 0.006$ vs M2 and $p = 0.018$ vs M3) during late stance and swing. During push-off and swing, the ankle dorsiflexion was larger (up to 8.0°, $p = 0.006$) for M2 compared to M1, while M1 had significantly outward pointing foot (up to 9.6°, $p = 0.006$). For M1 vs M2 and M3 the Cohen's effect size were medium ($d > 0.5$) for pelvis obliquity and ankle dorsiflexion, large ($d > 0.9$) for hip adduction and rotation and very large ($d > 1.2$) for foot progression. Very small ($d < 0.01$) values were found only for pelvis tilt and rotation. Conversely, small effect sizes were generally found for M2 vs M3, except for the ankle dorsiflexion ($d > 0.6$).

Correlations between thirty-six possible joint kinematics pairs were calculated for all models (full details in additional material Table A2). Table 2 presents the results for those eight pairs in which the ANOVA highlighted a significant difference between the models. Changes in the correlation strength were observed for most pairings when adopting the different models, with the most evident being: r (hip flexion, hip rotation) going from moderate (M2 and M3) to strong (M1); r (hip adduction, knee flexion) going from weak (M1) to moderate (M2 and M3); r (hip adduction, ankle dorsiflexion) going from weak (M2) to moderate (M1 and M3); r (knee flexion, foot progression) going from weak (M3) to moderate (M2) and strong (M1). The r (hip flexion, foot progression) became significant, although weak, in M2 and M3 and the same happened for r (ankle dorsiflexion, foot progression) in M1.

$\overline{RMSD}$ (individual $RMSD$ of the various DOFs in additional material, Table A3) values calculated from the different models differed for most participants, with M3 disagreeing with M1 and M2 when identifying the participants with the largest $\overline{RMSD}$ and all models disagreeing when identifying the participant with the smallest $\overline{RMSD}$ (Fig. 4). For example, participant 2 had the largest $\overline{RMSD}$ according to M1 and M2 (6.7° and 6.9°, respectively) but was amongst the smallest according to M3 (4.0°). Participant 9 had the largest $\overline{RMSD}$ (8.3°) based on M3 and the 5th largest $\overline{RMSD}$ (5.9°) based on M1 but had the 3rd smallest $\overline{RMSD}$ (3.9°) according to M2.

4. Discussion

By including three different ankle joint models in the same image-based skeletal model of the lower limb we showed for the first time that different definitions of ankle joint affect the estimates of proximal lower-limb kinematics. Notably, while the three models embedded the same dorsiflexion axis definition, they provided different dorsiflexion angles estimates. Even more interestingly, the differences generated by the ankle modelling also significantly affected the knee, hip and pelvis

Table 2
Results of analysis of correlations between different joint angles.

Correlated DOFs		Pearson's correlation coefficient r (mean ± SD)			Post-hoc
		M1	**M2**	**M3**	
Pelvis obliquity	**Hip adduction**	0.75 ± 0.27	0.82 ± 0.20	0.82 ± 0.21	*p12,p31* < 0.001
	Hip rotation	−0.70 ± 0.26	−0.60 ± 0.31	−0.51 ± 0.38	*p12* = 0.002; *p23, p31* < 0.001
Hip flexion	**Foot progression**	−0.21 ± 0.28	−0.38 ± 0.33	−0.41 ± 0.35	*p12,p31* < 0.001
	Knee flexion	−0.48 ± 0.15	−0.61 ± 0.09	−0.62 ± 0.09	*p23,p31* < 0.001
Hip adduction	**Ankle dorsiflexion**	0.54 ± 0.17	0.48 ± 0.24	0.64 ± 0.15	*p12,p31* < 0.001
	Foot progression	0.69 ± 0.22	0.56 ± 0.23	0.52 ± 0.25	*p12* = 0.002; p31 < 0.001
Knee flexion	**Foot progression**	−0.79 ± 0.12	−0.54 ± 0.28	−0.43 ± 0.31	*p12,p23, p31* < 0.001
Ankle dorsiflexion	**Foot progression**	0.46 ± 0.14	0.16 ± 0.21	0.15 ± 0.17	*p12,p31* < 0.001

Mean ± standard deviation (over the 15 available datasets) Pearson's correlation coefficient r obtained by correlating the listed DOFs in M1, M2 and M3, where S, M, W, and A stand for strong, moderate, weak, and absent, respectively and are highlighted with shades of green (positive correlation) or red (negative correlation). Column Post-hoc shows the p values of the significant post-hoc comparisons: *p12, p23* and *p31* referring to the comparisons between M1 and M2, M2 and M3, and M3 and M1, respectively.

kinematics, even if the changes of the latter had a very limited practical significance.

At group level, small, but statistically significant, differences between model outputs were found for most movements, with the largest differences observed for hip adduction and rotation, ankle dorsiflexion and foot progression. Overall M2 kinematics was similar to M3, except for up to 8.0° larger ankle dorsiflexion around push-off with M2. A possible explanation for this lies in the fact that M1 and M3 are mono-segment models, while M2 is a two-segment model. On the contrary, previous studies investigating the effect of using multi- versus mono-segment foot models, both in the context of marker-based gait analysis and MSK modelling (Malaquias et al., 2017; Pothrat et al., 2015; Stebbins et al., 2006; Zandbergen et al., 2020), reported significantly larger dorsiflexion (7.5 ± 1.2° over the gait cycle) for the mono-segment models. However, none of these studies used image-based personalisation to identify the anatomical axes. Additionally, M2 had an anatomical subtalar axis whose projection on the horizontal plane formed an acute angle with the tibiotalar axis, which could have led to a crosstalk between DOFs, with the subtalar joint capturing part of the foot dorsiflexion (Roach et al., 2016).

A heterogeneous response to the use of different models was observed for most joint angles across the participants, with minimal differences observed for pelvis tilt and rotations and the largest differences for the ankle dorsiflexion. Despite the ankle dorsiflexion having the most variation across participants between M1 and M2 (up to 18°), no statistical significance was observed at a group level due to the heterogeneity of the changes. A possible explanation for this can be found in the individual morphological characteristics of the talar bones of each participant, affecting the ankle axes identification. The orientation of tibiotalar and subtalar axes can vary by up to 30° and 48°, respectively, amongst healthy individuals (Isman et al., 1969), which, as previously reported (Montefiori et al., 2019), could justify the spread of the curves shown in Fig. 2. An additional role could be played by differences in individual walking pattern and experimental inaccuracy associated with the soft tissue artifacts. However, according to previous literature (Kainz et al., 2017b), experimental errors should affect Inverse Kinematics Tool outputs by no more than 3° for most limb DOFs (except for 5° errors for hip rotation). Therefore, our reported differences, which were above these values, were more likely arising from the individual characteristics. The differences between M1 and M2 average dorsiflexion curves found in this study were about 3° larger than those obtained by Kainz et al. (2017b) when comparing kinematics from one-DOF (equivalent to M1) and two-DOFs (equivalent to M2) generic-scaled models. A possible explanation could lie in the different knee joint model used by Kainz et al. (2017a) and in the larger foot marker set used in our study, allowing to better capture the non-sagittal movement and hence highlight differences between models. Lastly, the use of a generic-scaled model could have masked some of the differences in the anatomical joint axes due to individual bone morphology (Montefiori et al., 2019).

A previous experimental study highlighted a positive correlation between foot eversion and pelvis anterior tilt while standing (Khamis and Yizhar, 2007). In our study, M2 and M3 allowed for inversion/eversion while M1 forced the foot in a neutral inversion/eversion configuration, not allowing for either frontal or transverse plane movements. Despite this, no significant variations were observed in pelvis tilt kinematics when comparing the models. Significant variations were observed for the other joints, with smaller hip flexion and larger hip adduction and rotation for M1. This suggests that not tracking non-sagittal movements of the foot induced changes at the level of the hip, where non-sagittal movement are allowed by the ball-and-socket joint.

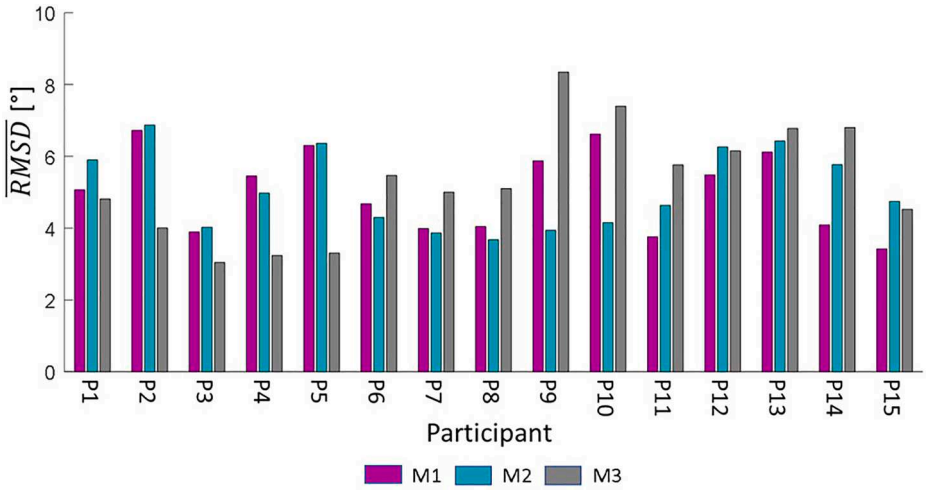

Fig. 4. Average root mean square deviation ($\overline{RMSD}$) obtained for each participant using M1 (fuchsia) M2 (turquoise) and M3 (grey).

Changes in correlation between joint kinematics have been previously used to discriminate between pathological and healthy populations (Chang et al., 2018; Lee and Wong, 2002; Pohl et al., 2006). The results here reported showed a strong correlation (0.75 with M1 and 0.82 with M2 and M3) between hip adduction and pelvis obliquity for all three models, confirming what previously reported (Deschamps et al., 2018; Lee and Wong, 2002). An interesting pattern was observed for M1, where the foot progression was more correlated than M2 and M3 with the ankle and the knee sagittal movements, but less with the hip angles. Limiting the ankle motion to the sagittal plane (M1) caused a larger hip internal rotation during late stance and a more outward pointing foot during push-off and initial swing. This suggests that ignoring ankle coronal and transverse motions has a greater effect on the transverse rotation of more proximal joints during stance and of the foot during swing. Similarly, changes in the coronal plane occur proximally in the first half of the gait cycle and distally in the second half. Additionally, stronger correlations between coronal and sagittal hip rotations were found for M1, which supports the conclusion that 1-DOF hinge ankle models induce crosstalk between joints and DOFs. Overall, the observed changes in correlation, due to the choice of a given model, could be erroneously associated with the presence of a pathological condition, potentially leading to wrong clinical interpretation of the data.

The RMSD is often used in the clinics to assess deviations between patients and reference control waveforms (Baker et al., 2009; Kainz et al., 2021). Previous research showed similarity in RMSD between cerebral palsy and typical developing children's when using MRI-based or generic models with the same joint DOFs and anatomical reference frame definitions (Kainz et al., 2021). Our results, however, indicate that changing ankle DOFs and joint axes orientation does indeed affect the kinematics of healthy participants, as proven by the fact that M1, M2 and M3 differently ranked the participants based on $\overline{RMSD}$. Given that a similar outcome should be expected when comparing pathological and control waveforms, this aspect should not be neglected when clinically interpreting output from a given kinematic model.

One of the limitations of this paper is that the analysis was confined to the most popular choices for modelling the ankle joint. Other more complex ankle models have been proposed, including those with six DOFs (Ding et al., 2019) and those based on anatomical congruence (Conconi and Castelli, 2014; Conconi et al., 2021), but we would expect also those to cause changes in the proximal lower-limb kinematics. More importantly, the choice of a simplified hinge knee joint, despite popular in the literature (Arnold et al., 2010; Delp et al., 1990; Rajagopal et al., 2016), likely affected the current finding by veiling possible alterations of knee motion in the other planes. A second important limitation is the lack of a validation dataset (i.e. dual fluoroscopy or dynamic MRI data), which did not allow to evaluate the best representation of the real ankle motion and associated proximal limb kinematics. The quantification of maximum marker tracking error (OpenSim Inverse Kinematics Tool) can represent a measure of the reliability of the models. Smaller errors found when increasing the ankle DOFs (M3) confirmed previous results from both generic-scaled and MRI-based models (Kainz et al., 2017b; Kainz et al., 2016), suggesting a better representation of the real foot movement when accounting for all foot rotations. On the contrary, a recent study reported a better match between ankle kinematics and dual fluoroscopy data when using one-DOF rather than three-DOF joint models (Nichols et al., 2016). Our study suggests that a comprehensive validation should ideally include all lower-limb joint kinematics instead of only focussing on ankle estimates to account for errors propagation to the proximal joints.

Even if the lack of a gold standard does not allow us to provide a definite answer toward the choice of the model to adopt, we believe that M2 should be preferred in the presence of abnormal joint anatomies. Among other critical factors, this would allow to avoid any risk of overestimating hip internal rotation and consequent femoral anteversion that might be associated with M1. This choice would be especially relevant in cerebral palsy where such models are largely adopted (Arnold and Delp, 2005; Kainz et al., 2017a; Kainz et al., 2017b; Kainz et al., 2021).

In conclusion, we confirmed the hypothesis that different definitions of ankle joint axes affect not only the ankle kinematics but, more interestingly, also that of the proximal joints. These variations can be substantial at individual level, hence potentially affecting the comparisons across studies or leading to erroneous clinical conclusions. This suggests that, even if only interested in studying the kinematics of a particular joint all the kinematic chain should be modelled consistently with the reference literature for the comparison to be meaningful. While modelling choices can be dictated by various factors, i.e. the purpose of the investigation and the data availability, generalisation of the results and their clinical meaningfulness should be made explicitly dependent on the consistency between methodologies. Future work will focus on understanding the effect of different ankle joint models on the estimate of muscle forces, particularly on the hip adductors and rotators. In fact, the differences in hip kinematics quantified in this study would suggest associated variations of muscle moment arm, hence affecting the muscle torque-generating capacity.

CRediT authorship contribution statement

Erica Montefiori: Writing – review & editing, Writing – original draft, Methodology, Investigation, Formal analysis, Data curation, Conceptualization, Visualization. **Claude Fiifi Hayford:** Writing – review & editing, Writing – original draft, Visualization, Supervision, Funding acquisition, Conceptualization. **Claudia Mazzà:** Writing – review & editing, Writing – original draft, Visualization, Supervision, Funding acquisition, Conceptualization.

Declaration of Competing Interest

The authors declare that they have no known competing financial interests or personal relationships that could have appeared to influence the work reported in this paper.

Acknowledgements

The data used for this study were collected as part of the European Commission "MD-Paedigree" programme (7th FP, Contract Number 600932). We are very grateful to the participants for their time and effort. The project is supported by the UK Engineering and Physical Sciences Research Council (EPSRC) (EP/K03877X/1 and EP/S032940/1), by the NIHR Sheffield Biomedical Research Centre (IS-BRC-1215-20017), and by the UK government Commonwealth Scholarship scheme. The views expressed are those of the authors and not necessarily those of the NHS, the NIHR or the Department of Health and Social Care.

Appendix A. Supplementary material

Supplementary data to this article can be found online at https://doi.org/10.1016/j.jbiomech.2022.111072. The models and input data used for this paper are available on Figshare at doi: 10.15131/shef.data.16831816

References

*Arnold *, A.S., Delp, S.L., 2005. Computer modeling of gait abnormalities in cerebral palsy: application to treatment planning. Theoret. Issues Ergon. Sci. 6 (3-4), 305–312.

Arnold, E.M., Ward, S.R., Lieber, R.L., Delp, S.L., 2010. A model of the lower limb for analysis of human movement. Ann. Biomed. Eng. 38 (2), 269–279.

Baker, R., McGinley, J.L., Schwartz, M.H., Beynon, S., Rozumalski, A., Graham, H.K., Tirosh, O., 2009. The gait profile score and movement analysis profile. Gait & posture 30 (3), 265–269.

Chang, S.-T., Lai, K.-L., Kuo, F.-C., Kao, Y.-S., 2018. Cross-correlation between spine and hip joint kinematics differs in healthy individuals and subgroups of ankylosing

spondylitis patients during trunk lateral flexion. Musculoskeletal Sci. Pract. 38, 8–14.
Cignoni, P., Callieri, M., Corsini, M., Dellepiane, M., Ganovelli, F., Ranzuglia, G., Year Meshlab: an open-source mesh processing tool. In Eurographics Italian chapter conference.
Conconi, M., Castelli, V.P., 2014. A sound and efficient measure of joint congruence. Proc. Inst. Mech. Eng. [H] 228 (9), 935–941.
Conconi, M., Montefiori, E., Sancisi, N., Mazzà, C., 2021. Modeling musculoskeletal dynamics during gait: evaluating the best personalization strategy through model anatomical consistency. Applied Sciences 11, 8348.
de Asla, R.J., Wan, L.u., Rubash, H.E., Li, G., 2006. Six DOF in vivo kinematics of the ankle joint complex: application of a combined dual-orthogonal fluoroscopic and magnetic resonance imaging technique. J. Orthop. Res. 24 (5), 1019–1027.
Delp, S.L., Anderson, F.C., Arnold, A.S., Loan, P., Habib, A., John, C.T., Guendelman, E., Thelen, D.G., 2007. OpenSim: open-source software to create and analyze dynamic simulations of movement. IEEE Trans. Biomed. Eng. 54, 1940–1950.
Delp, S.L., Loan, J.P., Hoy, M.G., Zajac, F.E., Topp, E.L., Rosen, J.M., 1990. An interactive graphics-based model of the lower extremity to study orthopaedic surgical procedures. IEEE Trans. Biomed. Eng. 37, 757–767.
Deschamps, K., Eerdekens, M., Geentjens, J., Santermans, L., Steurs, L., Dingenen, B., Thysen, M., Staes, F., 2018. A novel approach for the detection and exploration of joint coupling patterns in the lower limb kinetic chain. Gait & Posture 62, 372–377.
Ding, Z., Tsang, C.K., Nolte, D., Kedgley, A.E., Bull, A.M.J., 2019. Improving musculoskeletal model scaling using an anatomical atlas: the importance of gender and anthropometric similarity to quantify joint reaction forces. IEEE Trans. Biomed. Eng. 66 (12), 3444–3456.
Isman, R.E., Inman, V.T., Poor, P., 1969. Anthropometric studies of the human foot and ankle. Bull Prosthet Res 11, 129.
Kainz, H., Carty, C.P., Maine, S., Walsh, H.P., Lloyd, D.G., Modenese, L., 2017a. Effects of hip joint centre mislocation on gait kinematics of children with cerebral palsy calculated using patient-specific direct and inverse kinematic models. Gait & posture 57, 154–160.
Kainz, H., Graham, D., Edwards, J., Walsh, H.P., Maine, S., Boyd, R.N., Lloyd, D.G., Modenese, L., Carty, C.P., 2017b. Reliability of four models for clinical gait analysis. Gait Post. 54, 325–331.
Kainz, H., Modenese, L., Lloyd, D.G., Maine, S., Walsh, H.P.J., Carty, C.P., 2016. Joint kinematic calculation based on clinical direct kinematic versus inverse kinematic gait models. J. Biomech. 49 (9), 1658–1669.
Kainz, H., Wesseling, M., Jonkers, I., 2021. Generic scaled versus subject-specific models for the calculation of musculoskeletal loading in cerebral palsy gait: Effect of personalized musculoskeletal geometry outweighs the effect of personalized neural control. Clin. Biomech. 87, 105402.
Khamis, S., Yizhar, Z., 2007. Effect of feet hyperpronation on pelvic alignment in a standing position. Gait Post. 25 (1), 127–134.
Kleipool, R.P., Dahmen, J., Vuurberg, G., Oostra, R.-J., Blankevoort, L., Knupp, M., Stufkens, S.A.S., 2019. Study on the three-dimensional orientation of the posterior facet of the subtalar joint using simulated weight-bearing CT. J. Orthopaed. Res.® 37 (1), 197–204.
Lee, R.Y.W., Wong, T.K.T., 2002. Relationship between the movements of the lumbar spine and hip. Hum. Mov. Sci. 21 (4), 481–494.
Lenz, A.L., Strobel, M.A., Anderson, A.M., Fial, A.V., MacWilliams, B.A., Krzak, J.J., Kruger, K.M., 2021. Assignment of local coordinate systems and methods to calculate tibiotalar and subtalar kinematics: a systematic review. J. Biomech. 120, 110344.
Lu, T.-W., O'Connor, J.J., 1999. Bone position estimation from skin marker co-ordinates using global optimisation with joint constraints. J. Biomech. 32 (2), 129–134.
Maharaj, J.N., Kessler, S., Rainbow, M.J., D'Andrea, S.E., Konow, N., Kelly, L.A., Lichtwark, G.A., 2020. The reliability of foot and ankle bone and joint kinematics measured with biplanar videoradiography and manual scientific rotoscoping. Front. Bioeng. Biotechnol. 8, 106.
Malaquias, T.M., Silveira, C., Aerts, W., De Groote, F., Dereymaeker, G., Vander Sloten, J., Jonkers, I., 2017. Extended foot-ankle musculoskeletal models for application in movement analysis. Comput. Methods Biomech. Biomed. Eng. 20 (2), 153–159.
Modenese, L., Montefiori, E., Wang, A., Wesarg, S., Viceconti, M., Mazzà, C., 2018. Investigation of the dependence of joint contact forces on musculotendon parameters using a codified workflow for image-based modelling. J. Biomech. 73, 108–118.
Montefiori, E., Modenese, L., Di Marco, R., Magni-Manzoni, S., Malattia, C., Petrarca, M., Ronchetti, A., de Horatio, L.T., van Dijkhuizen, P., Wang, A., Wesarg, S., Viceconti, M., Mazzà, C., 2019. An image-based kinematic model of the tibiotalar and subtalar joints and its application to gait analysis in children with Juvenile Idiopathic Arthritis. J. Biomech. 85, 27–36.
Nichols, J.A., Roach, K.E., Fiorentino, N.M., Anderson, A.E., 2016. Predicting tibiotalar and subtalar joint angles from skin-marker data with dual-fluoroscopy as a reference standard. Gait & posture 49, 136–143.
Pataky, T.C., 2012. One-dimensional statistical parametric mapping in Python. Comput Methods Biomech Biomed Engin 15 (3), 295–301.
Pinto, R.Z.A., Souza, T.R., Trede, R.G., Kirkwood, R.N., Figueiredo, E.M., Fonseca, S.T., 2008. Bilateral and unilateral increases in calcaneal eversion affect pelvic alignment in standing position. Manual therapy 13 (6), 513–519.
Pohl, M.B., Messenger, N., Buckley, J.G., 2006. Changes in foot and lower limb coupling due to systematic variations in step width. Clin. Biomech. 21 (2), 175–183.
Pothrat, C., Authier, G., Viehweger, E., Berton, E., Rao, G., 2015. One-and multi-segment foot models lead to opposite results on ankle joint kinematics during gait: implications for clinical assessment. Clin. Biomech. 30 (5), 493–499.
Prinold, J.A.I., Mazzà, C., Di Marco, R., Hannah, I., Malattia, C., Magni-Manzoni, S., Petrarca, M., Ronchetti, A.B., Tanturri de Horatio, L., van Dijkhuizen, E.H.P., Wesarg, S., Viceconti, M., 2016. A patient-specific foot model for the estimate of ankle joint forces in patients with juvenile idiopathic arthritis. Ann. Biomed. Eng. 44 (1), 247–257.
Rajagopal, A., Dembia, C.L., DeMers, M.S., Delp, D.D., Hicks, J.L., Delp, S.L., 2016. Full-body musculoskeletal model for muscle-driven simulation of human gait. IEEE Trans. Biomed. Eng. 63 (10), 2068–2079.
Roach, K.E., Wang, B., Kapron, A.L., Fiorentino, N.M., Saltzman, C.L., Bo Foreman, K., Anderson, A.E., 2016. In vivo kinematics of the tibiotalar and subtalar joints in asymptomatic subjects: a high-speed dual fluoroscopy study. J. Biomech. Eng. 138.
Rutherford, D.J., Hubley-Kozey, C.L., Deluzio, K.J., Stanish, W.D., Dunbar, M., 2008. Foot progression angle and the knee adduction moment: a cross-sectional investigation in knee osteoarthritis. Osteoarthritis Cartilage 16 (8), 883–889.
Saraswat, P., Andersen, M.S., MacWilliams, B.A., 2010. A musculoskeletal foot model for clinical gait analysis. J. Biomech. 43 (9), 1645–1652.
Smith, D.K., Berquist, T.H., An, K.-N., Robb, R.A., Chao, E.Y.S., 1989. Validation of three-dimensional reconstructions of knee anatomy: CT vs MR imaging. J. Comput. Assist. Tomogr. 13 (2), 294–301.
Stebbins, J., Harrington, M., Thompson, N., Zavatsky, A., Theologis, T., 2006. Repeatability of a model for measuring multi-segment foot kinematics in children. Gait Post. 23 (4), 401–410.
Steger, S., Kirschner, M., Wesarg, S., Year Articulated atlas for segmentation of the skeleton from head & neck CT datasets. In 2012 9th IEEE International Symposium on Biomedical Imaging (ISBI).
Valente, G., Crimi, G., Vanella, N., Schileo, E., Taddei, F., 2017. nmsBuilder: freeware to create subject-specific musculoskeletal models for OpenSim. Comput. Methods Progr. Biomed. 152, 85–92.
van Sint Jan, S., 2007. Color atlas of skeletal landmark definitions E-book: Guidelines for reproducible manual and virtual palpations. Elsevier Health Sciences.
Wang, B., Roach, K.E., Kapron, A.L., Fiorentino, N.M., Saltzman, C.L., Singer, M., Anderson, A.E., 2015. Accuracy and feasibility of high-speed dual fluoroscopy and model-based tracking to measure in vivo ankle arthrokinematics. Gait Post. 41 (4), 888–893.
Wu, G.e., Siegler, S., Allard, P., Kirtley, C., Leardini, A., Rosenbaum, D., Whittle, M., D'Lima, D.D., Cristofolini, L., Witte, H., Schmid, O., Stokes, I., 2002. ISB recommendation on definitions of joint coordinate system of various joints for the reporting of human joint motion—part I: ankle, hip, and spine. J. Biomech. 35 (4), 543–548.
Zandbergen, M.A., Schallig, W., Stebbins, J.A., Harlaar, J., van der Krogt, M.M., 2020. The effect of mono-versus multi-segment musculoskeletal models of the foot on simulated triceps surae lengths in pathological and healthy gait. Gait Post. 77, 14–19.